

Observation of a Higher-Order Topological Bound State in the Continuum

Alexander Cerjan¹,* Marius Jürgensen¹, Wladimir A. Benalcazar¹,† Sebabrata Mukherjee¹, and Mikael C. Rechtsman¹‡
Department of Physics, The Pennsylvania State University, University Park, Pennsylvania 16802, USA

 (Received 27 June 2020; accepted 13 October 2020; published 17 November 2020)

Higher-order topological insulators are a recently discovered class of materials that can possess zero-dimensional localized states regardless of the dimension of the system. Here, we experimentally demonstrate that the topological corner-localized modes of higher-order topological systems can be symmetry-protected bound states in the continuum; these states do not hybridize with the surrounding bulk states of the lattice even in the absence of a bulk band gap. This observation expands the scope of bulk-boundary correspondence by showing that protected boundary-localized states can be found within topological bands, in addition to being found in between them.

DOI: [10.1103/PhysRevLett.125.213901](https://doi.org/10.1103/PhysRevLett.125.213901)

Topological materials have garnered significant interest for their ability to support boundary-localized states that manifest unusual phenomena, such as the backscatter-free chiral edge states found in quantum Hall systems [1–14], and edge-localized states found in systems with quantized dipole moments [15–17]. Recently, a new class of materials was discovered whose crystalline symmetries yield topological phases that can protect zero-dimensional corner-localized states in two dimensions or, more generally, $(d - n)$ -dimensional states at the boundaries of d -dimensional lattices, with $n \geq 2$ [18–32]. Coined higher-order topological insulators, if these systems are also chiral or particle-hole symmetric, their corner-localized states appear at the center of their energy spectrum. However, the crystalline symmetries that protect these phases do not necessarily imply the presence of a bulk band gap at this energy. This raises the question—do the corner-localized states remain exponentially localized despite being degenerate with the bulk bands, or do they hybridize with the bulk states and lose their spatial localization? If the state remains localized with an infinite lifetime, it is a bound state in the continuum (BIC) [33–40], where the continuum is formed by the bulk bands whose states extend throughout the infinite lattice; otherwise, the state is a standard resonance, where any energy initially added to the corner will eventually radiate away into the lattice with finite lifetime [41]. Recently, it was theoretically predicted that a higher-order topological phase can protect corner-localized BICs if the system satisfies additional symmetry requirements [42].

Finding a zero-dimensional BIC in a system whose topology is dependent upon only its crystalline symmetries presents a significant opportunity in two- and three-dimensional photonic crystals [43]. Such states could be used to realize cavities in low-index photonic crystals, where there are no known crystal designs which yield complete band gaps [44,45]. Although higher-order topological phases have been demonstrated in a wide range of different

physical platforms, including microwaves [46–48], photonics [49–53], acoustics [54–62], electric circuits [63,64], and atomic systems [65], all of these previous studies have been limited to systems analogous to insulators and exhibit spectrally isolated corner-localized states.

Here, we experimentally realize a higher-order topological bound state in the continuum using a two-dimensional array composed of evanescently coupled waveguides [66,67]. To show that our waveguide array possesses a BIC, we perform three separate experiments. First, by injecting light into the corner of the array, we prove that the lattice exhibits a corner-localized mode in its topological phase but not in its trivial phase. Second, by using an auxiliary waveguide to couple into the array, which fixes the effective energy of the initial excitation, we show that this corner-localized mode appears at the center of the spectrum and is degenerate with bulk states of the lattice. Finally, we show that our bound state transforms into a resonance when we break chiral symmetry by detuning the index of refraction of the members of one sublattice. Together, these experiments prove that the corner-localized state of our higher-order topological waveguide array is a symmetry-protected BIC and does not hybridize with the bulk bands so long as the necessary symmetries remain intact.

Our experimental system consists of a square lattice in which each unit cell contains four waveguides and is C_{4v} symmetric, as shown in Fig. 1(a) [28,42,68–70]. As each waveguide supports only a single bound mode that is evanescently coupled to neighboring waveguides (for the wavelengths we consider), our array can be approximated using a tight-binding model with only nearest-neighbor couplings, such that the lattice is chiral (sublattice) symmetric. The diffraction of light through the structure is governed by

$$i\partial_z|\psi(z, \lambda)\rangle = \hat{H}(\lambda)|\psi(z, \lambda)\rangle. \quad (1)$$

Here, $|\psi(z, \lambda)\rangle$ is the envelope of the electric field on each of the waveguides at propagation distance z and wavelength λ . The coupling coefficients t_{intra} and t_{inter} in \hat{H} are determined by the spacings between neighboring waveguides within the same unit cell, l_{intra} , and between adjacent unit cells, l_{inter} .

For an infinite array in the transverse plane, the Bloch Hamiltonian of the lattice can be written as

$$\frac{h(\mathbf{k})}{t_{\text{inter}}} = \begin{pmatrix} 0 & Q \\ Q^\dagger & 0 \end{pmatrix}, \quad Q = \begin{pmatrix} \gamma + e^{ik_x a} & \gamma + e^{ik_y a} \\ \gamma + e^{-ik_y a} & \gamma + e^{-ik_x a} \end{pmatrix}, \quad (2)$$

where a is the lattice constant, $\gamma = t_{\text{intra}}/t_{\text{inter}}$, and $\mathbf{k} = (k_x, k_y)$. To assist with comparisons with the topological literature, we refer to the eigenvalues of the waveguide array, \hat{H} , as energies E , with “zero energy” in the middle of this spectrum, while noting that physically these values correspond to shifts in the propagation constant $\beta = -E = k_z - k_0$ of $|\psi\rangle$ along the z axis. Here, $k_0 = \omega n_0/c$, where n_0 is the index of refraction of the borosilicate glass into which the waveguides are fabricated and ω is the frequency of the injected light.

The presence of C_{4v} symmetry in the lattice permits two distinct topological phases depending on the ratio of the spacings between neighboring waveguides within and between adjacent unit cells. In its topological phase $l_{\text{intra}}/l_{\text{inter}} > 1$, the bands possess different representations of C_{4v} (C_{2v}) at the corresponding high-symmetry points \mathbf{M} (\mathbf{X} and \mathbf{Y}) in the Brillouin zone than they do at Γ . However, in its trivial phase $l_{\text{intra}}/l_{\text{inter}} < 1$, each band possesses the same symmetry representation at all of the high-symmetry points. The topological phase transition occurs at $l_{\text{intra}}/l_{\text{inter}} = 1$, when the bulk band gap closes at the high-symmetry points, allowing for the bands to exchange their representations of these crystalline symmetries. In its topological phase, C_2 symmetry protects edge-localized states in the bulk band gaps and a corner-induced filling

anomaly [28,42]. In Fig. 1(b), the presence of these extra corner-localized states can be observed in the local density of states of the central bulk band of the finite lattice. Note that when l_{intra} is interchanged with l_{inter} , both the topological and trivial phases of the array have the same bulk band structure consisting of four bands, shown in Fig. 1(c). An example waveguide array is displayed in Fig. 1(d).

Because of C_{4v} and chiral symmetries, the lattice possesses gapless bulk bands at zero energy regardless of its topological phase. These same two symmetries also pin the corner-localized states to zero energy, guaranteeing that these states are degenerate with the bulk bands while simultaneously protecting them from hybridizing with these bulk states [42]. This protection comes in two parts. First, two combinations of the four corner states have incompatible symmetry representations with the bulk bands at zero energy and, thus, cannot hybridize with them. Then, the two remaining combinations of corner-localized states must be both rotationally symmetric partners, with the same energy, and chiral symmetric partners, with opposite energies, forcing their energies to remain pinned at zero. This prevents these two corner-localized states from hybridizing with the degenerate bulk states to change their energies or modal profiles, and as such any hybridization of the corner states with the bulk states is simply a change in basis that does not alter their underlying spatially localized nature. Thus, all four corner states are topologically guaranteed to be zero-dimensional symmetry-protected BICs. If a band gap were opened around the corner-localized states, for example, by turning on an effective magnetic field, they would instead become traditional bound states [19].

In our experiment, it is impossible to completely remove the next-nearest-neighbor couplings which exist in the array and break chiral symmetry. However, the decay length of the corner state due to this slight symmetry breaking (~ 25 m) is significantly longer than the propagation length in our experiments, $L = 7.6$ cm [71]. As such, our experimental array is effectively chiral symmetric.

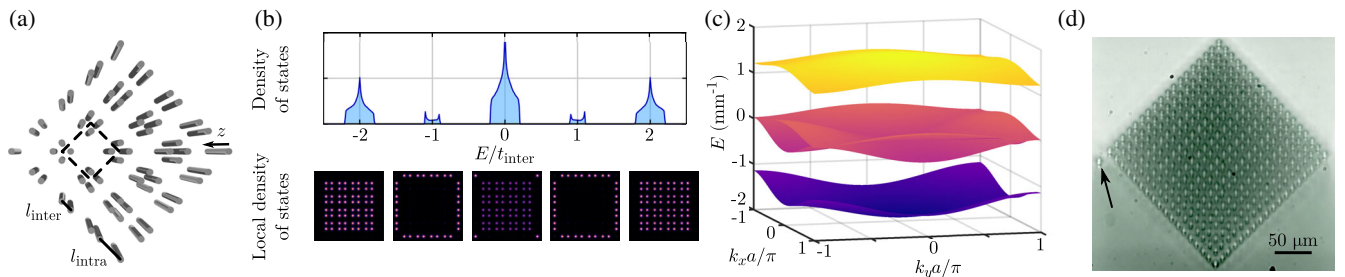


FIG. 1. (a) Schematic of a higher-order topological waveguide array. A unit cell is marked with a black dashed square. (b) Density of states (top panel) and associated local density of states (bottom panel) for each band of a finite lattice, calculated using the tight-binding approximation. (c) Bulk band structure for the higher-order topological waveguide array, calculated using full-wave numerical simulations for $\lambda = 850$ nm, $l_{\text{intra}} = 17$ μm , and $l_{\text{inter}} = 13$ μm . (d) White light transmission micrograph of the output facet of a waveguide array, with $l_{\text{intra}} = 13$ μm and $l_{\text{inter}} = 11$ μm . An auxiliary waveguide into which light can be injected is indicated with a black arrow.

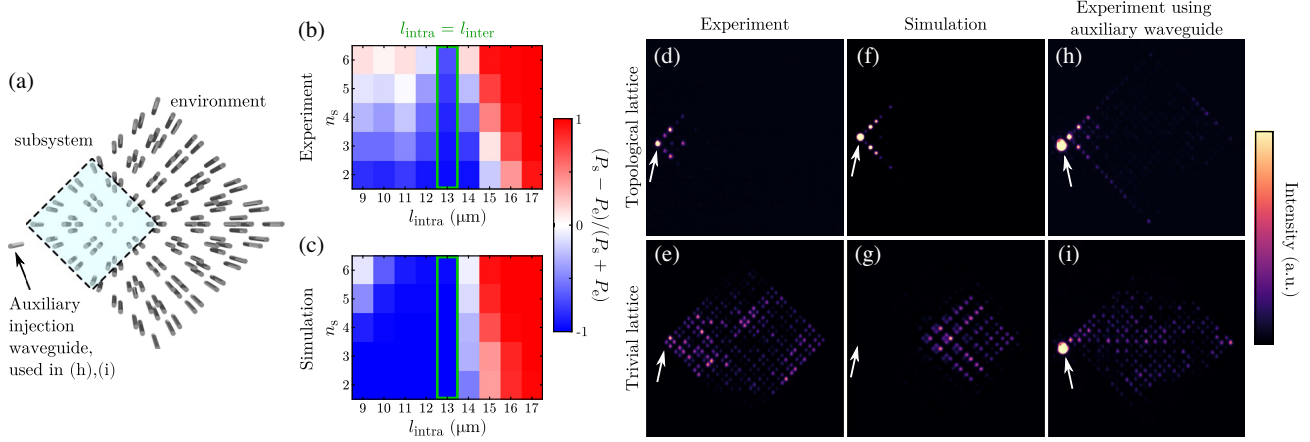


FIG. 2. (a) Schematic of a waveguide array with the boundary of the “subsystem” for $n_s = 3$ indicated. (b),(c) Experimentally observed (b) and numerically simulated (c) fractional power, as a function of the size of the subsystem, n_s , and the spacing between adjacent waveguides within the same unit cell, l_{intra} . We fix $l_{\text{inter}} = 13 \mu\text{m}$, and use $\lambda = 850 \text{ nm}$, with a propagation distance of $L = 7.6 \text{ cm}$. The arrays consist of 9×9 unit cells. The topological transition is denoted in green at $l_{\text{intra}} = l_{\text{inter}} = 13 \mu\text{m}$. (d),(e) Experimentally observed intensity for $l_{\text{intra}} = 17 \mu\text{m}$ (d) and $l_{\text{intra}} = 9 \mu\text{m}$ (e). Light is injected into the leftmost waveguide at the corner of the array, marked with a white arrow. (f),(g) The same as (d),(e), except for full wave numerical simulations of the waveguide array. (h) Experimentally observed intensity for a topological array, with $l_{\text{intra}} = 13 \mu\text{m}$ and $l_{\text{inter}} = 11 \mu\text{m}$, with wavelength $\lambda = 900 \text{ nm}$ and propagation distance $L = 7.6 \text{ cm}$. Light is injected using an auxiliary waveguide placed $20 \mu\text{m}$ away from the corner of the lattice (marked with a white arrow). (i) The same as (h) except with $l_{\text{intra}} = 11 \mu\text{m}$ and $l_{\text{inter}} = 13 \mu\text{m}$.

Previous studies of systems supporting BICs have identified that separability, the possibility to write \hat{H} as $\hat{H}(\mathbf{r}) = \hat{H}_x(x) + \hat{H}_y(y)$, can also protect BICs [34]. Nevertheless, despite the fact that Eq. (2) is separable, separability is *not* what protects the higher-order topological BICs we consider here. Analytically, one still observes higher-order topological BICs when additional terms have been added to the lattice’s Hamiltonian which obey C_{4v} and chiral symmetries but break separability [42,71].

To experimentally prove that our waveguide array contains a higher-order topological BIC, we first inject light into the corner of the array and observe whether most of the light remains confined to this corner or diffracts into the bulk. To assess the localization of the light at the output facet of the array, we divide the array into two regions, the “subsystem” which represents the square of unit cells with side length n_s closest to the corner, as indicated in Fig. 2(a), while the remaining waveguides comprise the “environment.” We then compare the total output power observed in the subsystem, P_s , with that of the environment, P_e , via $(P_s - P_e)/(P_s + P_e)$. For this “fractional power,” values near $+1$ correspond to the output power being localized in the subsystem, while values near -1 indicate that the wave function has diffracted into the environment. Although the exponential tail of the BIC can yield a fractional power < 1 for small values of n_s , especially when l_{inter} is only slightly larger than l_{intra} , in an infinite topological array a BIC will always exhibit a fractional power ~ 1 for a sufficiently large but finite n_s , while no state in a trivial array ever will.

As can be seen in Figs. 2(b) and 2(c), the wave function remains localized to the subsystem, until the topological

phase transition $l_{\text{intra}}/l_{\text{inter}} = 1$. The observed intensity at the output facet is shown for an example of both the topological and trivial arrays in Figs. 2(d)–2(g). Note that the increase seen in the fractional power for large subsystem sizes for some topologically trivial arrays is due to spurious reflections off of some of the waveguides at the top and bottom of the array due to fabrication imperfections, as well as reflections off of the far side of the array. Nevertheless, it is clear from Fig. 2(e) that these arrays do not possess a bound state. Thus, these results indicate that the waveguide array possesses a bound state in its topological phase but do not yet prove that the bound state is degenerate with the surrounding bulk bands.

To prove that this topological bound state is a BIC, we inject light into the waveguide array using an auxiliary waveguide weakly coupled to the lattice and placed near one of the corners. Since this waveguide is identical to those in the lattice, it effectively acts as a fixed zero-energy source that can excite only spatially overlapping states near zero energy in the array. Thus, when the array is in its topological phase [Fig. 2(h)], the dominant excited mode is the topological corner-localized mode, though bulk modes can still be excited. However, when l_{intra} and l_{inter} are reversed [Fig. 2(i)], the bulk of the lattice remains completely unchanged, but the array is now in the trivial phase. Upon excitation using an auxiliary waveguide, we see that bulk states of the lattice are excited, and there is no corner-localized mode. Since the lattice bulk is identical in both cases, this proves that there are zero-energy bulk states which are degenerate with the topological corner-localized state, and, thus, the corner-localized state is a BIC.

Finally, to demonstrate that this higher-order topological BIC is protected by chiral symmetry, we purposefully break chiral symmetry by increasing the refractive index on two of the four waveguides in each unit cell, as indicated in Fig. 3(a), which decreases the effective on-site energy of these two lattice sites. This has several consequences for the array. First, this opens a bulk band gap in the center of the spectrum; one of the two central bulk bands remains at zero energy (which is no longer at the middle of the spectrum), while the other's energy decreases, as shown in Fig. 3(b). Second, as each corner-localized state has support on only two of the four waveguides in the unit cell (diagonally across from one another), this change also breaks the fourfold degeneracy of the corner-localized states. Instead, the two corner-localized states with support on the perturbation decrease their energy, remaining degenerate with the lower energy of the two central bulk bands, while the other pair of corner-localized states remain degenerate with the bulk band at zero energy, as shown in Fig. 3(c). Although the topological corner-localized modes are still associated with a filling anomaly, now that chiral symmetry has been broken, these states are allowed to hybridize with bulk states, transforming from BICs into resonances.

We can observe this transition of one of the BICs into a resonance by incrementally increasing the strength of the sublattice symmetry breaking and coupling into the lattice using an auxiliary waveguide, which remains at zero energy, as shown in Figs. 3(d)–3(h). As chiral symmetry

is lost [Figs. 3(e)–3(h)], the wave function within the array begins to disassociate from the corner, and the maximum of this wave function travels into the bulk of the array and along the edges, signifying that all of the states being excited by the auxiliary waveguide have significant spatial overlap with the other modes of the lattice. In other words, the corner-localized state has become a resonance and is no longer a BIC. This is in clear contrast to what is seen in Fig. 3(d), where chiral symmetry is intact and the wave function in the lattice remains localized to the corner, indicating the presence of a BIC.

In conclusion, we have experimentally observed a higher-order topological bound state in the continuum in a waveguide array. This BIC is protected by C_{4v} and chiral symmetries and is topologically guaranteed to exist at the center of the spectrum. Moreover, as these states are able to confine light to a zero-dimensional mode in the absence of a bulk band gap, this provides a potential mechanism for creating cavities in low-index photonic systems that are unable to support complete band gaps. In particular, this means that, in principle, higher-order topological BICs could be used to confine light in photonic systems fabricated using two-photon lithography in photoresist [77,78], or colloids [79], which are typically composed of materials with refractive indices $n \sim 1.5$, though additional developments would be necessary to realize such BICs in these systems. We expect that zero-dimensional bound states in the continuum of the kind described here

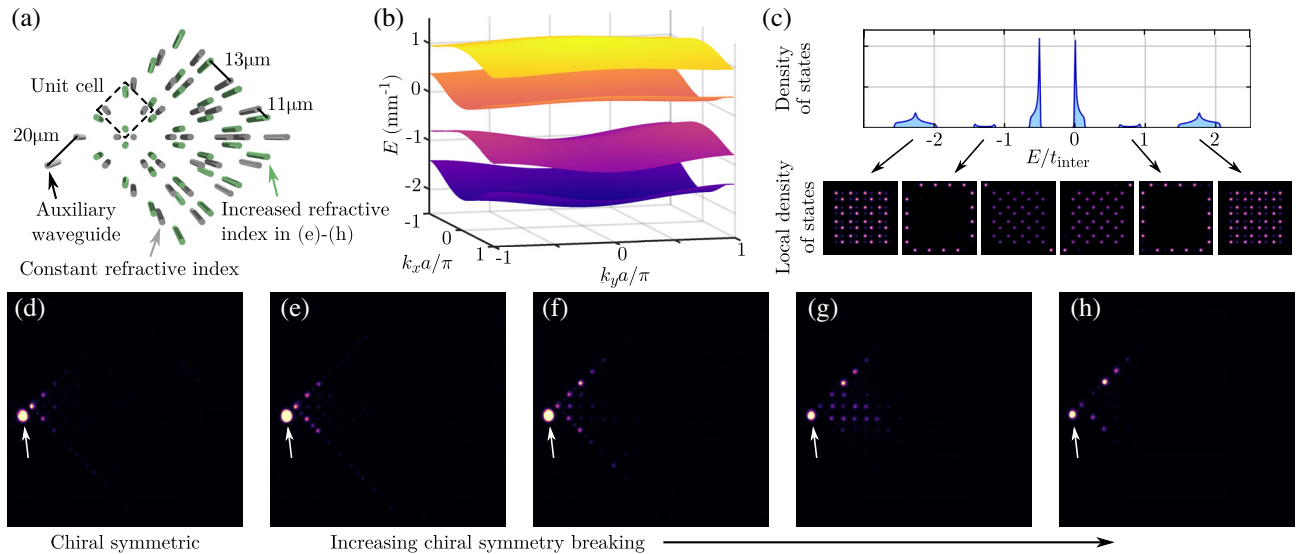


FIG. 3. (a) Schematic of a higher-order topological waveguide array with broken chiral symmetry, with an auxiliary waveguide $20 \mu\text{m}$ away from the array. Green colored waveguides were fabricated using slower writing speeds, resulting in a larger refractive index (decreased on-site energy). (b) Bulk band structure for the higher-order topological array with broken chiral symmetry, calculated using full-wave numerical simulations for $\lambda = 900 \text{ nm}$, $l_{\text{intra}} = 13 \mu\text{m}$, and $l_{\text{inter}} = 11 \mu\text{m}$, corresponding to the results shown in (f), below [71]. (c) Density of states (top panel) and associated local density of states for each band (bottom panel) for a tight-binding lattice with broken chiral symmetry. Zero energy of the chiral symmetric array is marked. (d) Experimentally observed intensity of the chiral symmetric array consisting of 9×9 unit cells, with $l_{\text{intra}} = 13 \mu\text{m}$, $l_{\text{inter}} = 11 \mu\text{m}$, and $\lambda = 900 \text{ nm}$, and propagation distance $L = 7.6 \text{ cm}$. The auxiliary waveguide where light is injected is marked with a white arrow. (e)–(h) Similar to (d), except with increasing the refractive index of the indicated sublattice of the array [71].

will lead to an expanded range of devices in which cavity and defect modes, for enhancing light-matter coupling, can be found.

This work was supported by the U.S. Office of Naval Research (ONR) Multidisciplinary University Research Initiative (MURI) Grant No. N00014-20-1-2325 on Robust Photonic Materials with High-Order Topological Protection, the ONR Young Investigator Award under Grant No. N00014-18-1-2595 as well as the Packard Foundation under Fellowship No. 2017-66821. W. A. B. acknowledges the support of the Eberly Postdoctoral Fellowship at the Pennsylvania State University. M. J. acknowledges the support of the Verne M. Willaman Distinguished Graduate Fellowship at the Pennsylvania State University. Computations for this research were performed on the Pennsylvania State University's Institute for Computational and Data Sciences' Roar supercomputer.

*awc19@psu.edu

†wxb151@psu.edu

‡mcrworld@psu.edu

- [1] K. v. Klitzing, G. Dorda, and M. Pepper, New Method for High-Accuracy Determination of the Fine-Structure Constant Based on Quantized Hall Resistance, *Phys. Rev. Lett.* **45**, 494 (1980).
- [2] B. I. Halperin, Quantized Hall conductance, current-carrying edge states, and the existence of extended states in a two-dimensional disordered potential, *Phys. Rev. B* **25**, 2185 (1982).
- [3] D. J. Thouless, M. Kohmoto, M. P. Nightingale, and M. den Nijs, Quantized Hall Conductance in a Two-Dimensional Periodic Potential, *Phys. Rev. Lett.* **49**, 405 (1982).
- [4] M. Büttiker, Absence of backscattering in the quantum Hall effect in multiprobe conductors, *Phys. Rev. B* **38**, 9375 (1988).
- [5] F. D. M. Haldane, Model for a Quantum Hall Effect without Landau Levels: Condensed-Matter Realization of the "Parity Anomaly," *Phys. Rev. Lett.* **61**, 2015 (1988).
- [6] F. D. M. Haldane and S. Raghu, Possible Realization of Directional Optical Waveguides in Photonic Crystals with Broken Time-Reversal Symmetry, *Phys. Rev. Lett.* **100**, 013904 (2008).
- [7] Z. Wang, Y. Chong, J. D. Joannopoulos, and M. Soljačić, Observation of unidirectional backscattering-immune topological electromagnetic states, *Nature (London)* **461**, 772 (2009).
- [8] R. O. Umucalılar and I. Carusotto, Artificial gauge field for photons in coupled cavity arrays, *Phys. Rev. A* **84**, 043804 (2011).
- [9] M. Hafezi, E. A. Demler, M. D. Lukin, and J. M. Taylor, Robust optical delay lines with topological protection, *Nat. Phys.* **7**, 907 (2011).
- [10] K. Fang, Z. Yu, and S. Fan, Realizing effective magnetic field for photons by controlling the phase of dynamic modulation, *Nat. Photonics* **6**, 782 (2012).
- [11] T. Kitagawa, M. A. Broome, A. Fedrizzi, M. S. Rudner, E. Berg, I. Kassal, A. Aspuru-Guzik, E. Demler, and A. G. White, Observation of topologically protected bound states in photonic quantum walks, *Nat. Commun.* **3**, 882 (2012).
- [12] M. C. Rechtsman, J. M. Zeuner, Y. Plotnik, Y. Lumer, D. Podolsky, F. Dreisow, S. Nolte, M. Segev, and A. Szameit, Photonic Floquet topological insulators, *Nature (London)* **496**, 196 (2013).
- [13] A. B. Khanikaev, S. H. Mousavi, W.-K. Tse, M. Kargarian, A. H. MacDonald, and G. Shvets, Photonic topological insulators, *Nat. Mater.* **12**, 233 (2013).
- [14] M. Hafezi, S. Mittal, J. Fan, A. Migdall, and J. M. Taylor, Imaging topological edge states in silicon photonics, *Nat. Photonics* **7**, 1001 (2013).
- [15] W. P. Su, J. R. Schrieffer, and A. J. Heeger, Solitons in Polyacetylene, *Phys. Rev. Lett.* **42**, 1698 (1979).
- [16] R. D. King-Smith and D. Vanderbilt, Theory of polarization of crystalline solids, *Phys. Rev. B* **47**, 1651 (1993).
- [17] J. Zak, Berrys Phase for Energy Bands in Solids, *Phys. Rev. Lett.* **62**, 2747 (1989).
- [18] W. A. Benalcazar, J. C. Y. Teo, and T. L. Hughes, Classification of two-dimensional topological crystalline superconductors and Majorana bound states at disclinations, *Phys. Rev. B* **89**, 224503 (2014).
- [19] W. A. Benalcazar, B. A. Bernevig, and T. L. Hughes, Quantized electric multipole insulators, *Science* **357**, 61 (2017).
- [20] W. A. Benalcazar, B. A. Bernevig, and T. L. Hughes, Electric multipole moments, topological multipole moment pumping, and chiral hinge states in crystalline insulators, *Phys. Rev. B* **96**, 245115 (2017).
- [21] Z. Song, Z. Fang, and C. Fang, $(d-2)$ -dimensional Edge States of Rotation Symmetry Protected Topological States, *Phys. Rev. Lett.* **119**, 246402 (2017).
- [22] J. Langbehn, Y. Peng, L. Trifunovic, F. von Oppen, and P. W. Brouwer, Reflection-Symmetric Second-Order Topological Insulators and Superconductors, *Phys. Rev. Lett.* **119**, 246401 (2017).
- [23] F. Schindler, A. M. Cook, M. G. Vergniory, Z. Wang, S. S. P. Parkin, B. A. Bernevig, and T. Neupert, Higher-order topological insulators, *Sci. Adv.* **4**, eaat0346 (2018).
- [24] O. Zilberberg, S. Huang, J. Guglielmon, M. Wang, K. P. Chen, Y. E. Kraus, and M. C. Rechtsman, Photonic topological boundary pumping as a probe of 4d quantum hall physics, *Nature (London)* **553**, 59 (2018).
- [25] B. J. Wieder and B. A. Bernevig, The axion insulator as a pump of fragile topology, arXiv:1810.02373.
- [26] G. van Miert and C. Ortix, Higher-order topological insulators protected by inversion and rotoinversion symmetries, *Phys. Rev. B* **98**, 081110(R) (2018).
- [27] M. Ezawa, Minimal models for wannier-type higher-order topological insulators and phosphorene, *Phys. Rev. B* **98**, 045125 (2018).
- [28] W. A. Benalcazar, T. Li, and T. L. Hughes, Quantization of fractional corner charge in C_n -symmetric higher-order topological crystalline insulators, *Phys. Rev. B* **99**, 245151 (2019).
- [29] E. Lee, R. Kim, J. Ahn, and B.-J. Yang, Two-dimensional higher-order topology in monolayer graphdiyne, *npj Quantum Mater.* **5**, 1 (2020).
- [30] X.-L. Sheng, C. Chen, H. Liu, Z. Chen, Y. X. Zhao, Z.-M. Yu, and S. A. Yang, Two-Dimensional Second-Order Topo-

- logical Insulator in Graphdiyne, *Phys. Rev. Lett.* **123**, 256402 (2019).
- [31] F. Schindler, M. Brzezińska, W. A. Benalcazar, M. Iraola, A. Bouhon, S. S. Tsirkin, M. G. Vergniory, and T. Neupert, Fractional corner charges in spin-orbit coupled crystals, *Phys. Rev. Research* **1**, 033074 (2019).
- [32] I. Petrides and O. Zilberberg, Higher-order topological insulators, topological pumps and the quantum Hall effect in high dimensions, *Phys. Rev. Research* **2**, 022049 (2020).
- [33] J. von Neumann and E. Wigner, Über merkwürdige diskrete eigenwerte, *Phys. Z.* **30**, 465 (1929).
- [34] C. W. Hsu, B. Zhen, A. D. Stone, J. D. Joannopoulos, and M. Soljačić, Bound states in the continuum, *Nat. Rev. Mater.* **1**, 16048 (2016).
- [35] H. Friedrich and D. Wintgen, Interfering resonances and bound states in the continuum, *Phys. Rev. A* **32**, 3231 (1985).
- [36] Y. Plotnik, O. Peleg, F. Dreisow, M. Heinrich, S. Nolte, A. Szameit, and M. Segev, Experimental Observation of Optical Bound States in the Continuum, *Phys. Rev. Lett.* **107**, 183901 (2011).
- [37] S. Weimann, Y. Xu, R. Keil, A. E. Miroschnichenko, A. Tünnermann, S. Nolte, A. A. Sukhorukov, A. Szameit, and Y. S. Kivshar, Compact Surface Fano States Embedded in the Continuum of Waveguide Arrays, *Phys. Rev. Lett.* **111**, 240403 (2013).
- [38] C. W. Hsu, B. Zhen, J. Lee, S.-L. Chua, S. G. Johnson, J. D. Joannopoulos, and M. Soljačić, Observation of trapped light within the radiation continuum, *Nature (London)* **499**, 188 (2013).
- [39] H. Zhou, B. Zhen, C. W. Hsu, O. D. Miller, S. G. Johnson, J. D. Joannopoulos, and M. Soljačić, Perfect single-sided radiation and absorption without mirrors, *Optica* **3**, 1079 (2016).
- [40] A. Cerjan, C. W. Hsu, and M. C. Rechtsman, Bound States in the Continuum through Environmental Design, *Phys. Rev. Lett.* **123**, 023902 (2019).
- [41] D. L. Bergman and G. Refael, Bulk metals with helical surface states, *Phys. Rev. B* **82**, 195417 (2010).
- [42] W. A. Benalcazar and A. Cerjan, Bound states in the continuum of higher-order topological insulators, *Phys. Rev. B* **101**, 161116(R) (2020).
- [43] J. D. Joannopoulos, S. G. Johnson, J. N. Winn, and R. D. Meade, *Photonic Crystals: Molding the Flow of Light*, 2nd ed. (Princeton University Press, Princeton, NJ, 2011).
- [44] H. Men, K. Y. K. Lee, R. M. Freund, J. Peraire, and S. G. Johnson, Robust topology optimization of three-dimensional photonic-crystal band-gap structures, *Opt. Express* **22**, 22632 (2014).
- [45] A. Cerjan and S. Fan, Complete photonic band gaps in supercell photonic crystals, *Phys. Rev. A* **96**, 051802(R) (2017).
- [46] C. W. Peterson, W. A. Benalcazar, T. L. Hughes, and G. Bahl, A quantized microwave quadrupole insulator with topologically protected corner states, *Nature (London)* **555**, 346 (2018).
- [47] X.-D. Chen, W.-M. Deng, F.-L. Shi, F.-L. Zhao, M. Chen, and J.-W. Dong, Direct Observation of Corner States in Second-Order Topological Photonic Crystal Slabs, *Phys. Rev. Lett.* **122**, 233902 (2019).
- [48] B.-Y. Xie, G.-X. Su, H.-F. Wang, H. Su, X.-P. Shen, P. Zhan, M.-H. Lu, Z.-L. Wang, and Y.-F. Chen, Visualization of Higher-Order Topological Insulating Phases in Two-Dimensional Dielectric Photonic Crystals, *Phys. Rev. Lett.* **122**, 233903 (2019).
- [49] J. Noh, W. A. Benalcazar, S. Huang, M. J. Collins, K. P. Chen, T. L. Hughes, and M. C. Rechtsman, Topological protection of photonic mid-gap defect modes, *Nat. Photonics* **12**, 408 (2018).
- [50] S. Mittal, V. V. Orre, G. Zhu, M. A. Gorlach, A. Poddubny, and M. Hafezi, Photonic quadrupole topological phases, *Nat. Photonics* **13**, 692 (2019).
- [51] Y. Ota, F. Liu, R. Katsumi, K. Watanabe, K. Wakabayashi, Y. Arakawa, and S. Iwamoto, Photonic crystal nanocavity based on a topological corner state, *Optica* **6**, 786 (2019).
- [52] M. Li, D. Zhirihin, M. Gorlach, X. Ni, D. Filonov, A. Slobozhanyuk, A. Alù, and A. B. Khanikaev, Higher-order topological states in photonic kagome crystals with long-range interactions, *Nat. Photonics* **14**, 89 (2020).
- [53] W. Zhang, X. Xie, H. Hao, J. Dang, S. Xiao, S. Shi, H. Ni, Z. Niu, C. Wang, K. Jin, X. Zhang, and X. Xu, Low-threshold topological nanolasers based on the second-order corner state, *Light Sci. Appl.* **9**, 109 (2020).
- [54] M. Serra-Garcia, V. Peri, R. Süsstrunk, O. R. Bilal, T. Larsen, L. Guillermo Villanueva, and S. D. Huber, Observation of a phononic quadrupole topological insulator, *Nature (London)* **555**, 342 (2018).
- [55] X. Ni, M. Weiner, A. Alù, and A. B. Khanikaev, Observation of higher-order topological acoustic states protected by generalized chiral symmetry, *Nat. Mater.* **18**, 113 (2019).
- [56] H. Xue, Y. Yang, F. Gao, Y. Chong, and B. Zhang, Acoustic higher-order topological insulator on a kagome lattice, *Nat. Mater.* **18**, 108 (2019).
- [57] H. Xue, Y. Yang, G. Liu, F. Gao, Y. Chong, and B. Zhang, Realization of an Acoustic Third-Order Topological Insulator, *Phys. Rev. Lett.* **122**, 244301 (2019).
- [58] X. Ni, M. Li, M. Weiner, A. Alù, and A. B. Khanikaev, Demonstration of a quantized acoustic octupole topological insulator, *Nat. Commun.* **11**, 2108 (2020).
- [59] X. Zhang, H.-X. Wang, Z.-K. Lin, Y. Tian, B. Xie, M.-H. Lu, Y.-F. Chen, and J.-H. Jiang, Second-order topology and multidimensional topological transitions in sonic crystals, *Nat. Phys.* **15**, 582 (2019).
- [60] X. Zhang, B.-Y. Xie, H.-F. Wang, X. Xu, Y. Tian, J.-H. Jiang, M.-H. Lu, and Y.-F. Chen, Dimensional hierarchy of higher-order topology in three-dimensional sonic crystals, *Nat. Commun.* **10**, 5331 (2019).
- [61] H. Xue, Y. Ge, H.-X. Sun, Q. Wang, D. Jia, Y.-J. Guan, S.-Q. Yuan, Y. Chong, and B. Zhang, Observation of an acoustic octupole topological insulator, *Nat. Commun.* **11**, 2442 (2020).
- [62] X. Zhang, Z.-K. Lin, H.-X. Wang, Z. Xiong, Y. Tian, M.-H. Lu, Y.-F. Chen, and J.-H. Jiang, Symmetry-protected hierarchy of anomalous multipole topological band gaps in nonsymmorphic metacrystals, *Nat. Commun.* **11**, 65 (2020).
- [63] S. Imhof, C. Berger, F. Bayer, J. Brehm, L. W. Molenkamp, T. Kiessling, F. Schindler, C. H. Lee, M. Greiter, T. Neupert, and R. Thomale, Topoelectrical-circuit realization of topological corner modes, *Nat. Phys.* **14**, 925 (2018).

- [64] J. Bao, D. Zou, W. Zhang, W. He, H. Sun, and X. Zhang, Topoelectrical circuit octupole insulator with topologically protected corner states, *Phys. Rev. B* **100**, 201406(R) (2019).
- [65] S. N. Kempkes, M. R. Slot, J. J. van den Broeke, P. Capiod, W. A. Benalcazar, D. Vanmaekelbergh, D. Bercioux, I. Swart, and C. M. Smith, Robust zero-energy modes in an electronic higher-order topological insulator, *Nat. Mater.* **18**, 1292 (2019).
- [66] K. M. Davis, K. Miura, N. Sugimoto, and K. Hirao, Writing waveguides in glass with a femtosecond laser, *Opt. Lett.* **21**, 1729 (1996).
- [67] A. Szameit and S. Nolte, Discrete optics in femtosecond-laser-written photonic structures, *J. Phys. B* **43**, 163001 (2010).
- [68] F. Liu and K. Wakabayashi, Novel Topological Phase with a Zero Berry Curvature, *Phys. Rev. Lett.* **118**, 076803 (2017).
- [69] M. Di Liberto, A. Recati, I. Carusotto, and C. Menotti, Two-body physics in the Su-Schrieffer-Heeger model, *Phys. Rev. A* **94**, 062704 (2016).
- [70] Z.-G. Chen, C. Xu, R. Al Jahdali, J. Mei, and Y. Wu, Corner states in a second-order acoustic topological insulator as bound states in the continuum, *Phys. Rev. B* **100**, 075120 (2019).
- [71] See Supplemental Material at <http://link.aps.org/supplemental/10.1103/PhysRevLett.125.213901> for a discussion of the methods used to fabricate the waveguide array, as well as the associated simulation parameters, a demonstration that separability is not what protects the BIC we observe here, and a discussion of the decay lengths of our BIC due to chiral symmetry breaking in our system, which includes Refs. [72–76].
- [72] Hermann A. Haus, *Waves and Fields in Optoelectronics* (Prentice Hall, Englewood Cliffs, NJ, 1983).
- [73] W. v. Ignatowsky, Reflexion elektromagnetischer Wellen an einem Draht, *Ann. Phys. (Leipzig)* **323**, 495 (1905).
- [74] D. M. Èidus, On the principle of limiting absorption, *Mat. Sb. (N.S.)* **57(99)**, 13 (1962), http://www.mathnet.ru/php/archive.phtml?wshow=paper&jrnid=sm&paperid=4636&option_lang=eng.
- [75] J. R. Schulenberger and C. H. Wilcox, The limiting absorption principle and spectral theory for steady-state wave propagation in inhomogeneous anisotropic media, *Arch. Ration. Mech. Anal.* **41**, 46 (1971).
- [76] A. Cerjan and A. D. Stone, Why the laser linewidth is so narrow: A modern perspective, *Phys. Scr.* **91**, 013003 (2016).
- [77] G. von Freymann, A. Ledermann, M. Thiel, I. Staude, S. Essig, K. Busch, and M. Wegener, Three-dimensional nanostructures for photonics, *Adv. Funct. Mater.* **20**, 1038 (2010).
- [78] T. Bückmann, N. Stenger, M. Kadic, J. Kaschke, A. Frölich, T. Kennerknecht, C. Eberl, M. Thiel, and M. Wegener, Tailored 3D mechanical metamaterials made by dip-in direct-laser-writing optical lithography, *Adv. Mater.* **24**, 2710 (2012).
- [79] D. J. Norris, E. G. Arlinghaus, L. Meng, R. Heiny, and L. E. Scriven, Opaline photonic crystals: How does self-assembly work? *Adv. Mater.* **16**, 1393 (2004).